Electromagnetic Science
vol. 2, no. 2, 0060182, June 2024
https://doi.org/10.23919/emsci.2024.0018

Research Article

Improving Radiation Pattern Roundness of Henge-Like Metaring-Loaded Monopoles Above a Finite Ground for MIMO Systems

Bo Zhang[1], Zhi Ning Chen[1], Yucong Zhou[2], Qun Lou[1], Jiahao Wang[1], and Koen Mouthaan[1]

1. *Department of Electrical and Computer Engineering*, *National University of Singapore*, *Singapore 117583*, *Singapore*
2. *Huawei Technologies Co.*, *Ltd.*, *Shenzhen 518129*, *China*

Corresponding author: Zhi Ning Chen, Email: eleczn@nus.edu.sg.
Received April 2, 2024; Accepted June 17, 2024; Published Online June 27, 2024.

Abstract — A henge-like metaring (HMR) is proposed for improving the radiation pattern roundness of monopole antennas off-center mounted on a finite ground by localizing the radiation from the monopole and suppressing the scattering by the ground. The improved patterns enhance uniform coverage of multiple-input and multiple-output (MIMO) systems. The study reveals that the radiation pattern of an off-center monopole is distorted by the asymmetric ground currents excited by both the feed and the radiation of the monopole. The distorted radiation patterns severely degrade wireless communication link quality. The HMR, composed of an annular array of mushroom unit cells, simultaneously functions as an electromagnetic bandgap (EBG) and a radiator, and encircles the monopole to form a henge monopole antenna (HMA). The HMR as an EBG is used to suppress the ground currents outside the HMR analyzed by an equivalent circuit model. The HMR as a radiator is designed to decouple the monopole from the ground with its elevated radiation pattern using characteristic mode analysis. As examples, two prototypes of single and four off-center MIMO HMAs are designed and investigated in the 2.45-GHz band. Simulated and measured results show that the single HMA and each of the four HMAs achieve the un-roundness of the radiation pattern at $\theta = 65°$ plane lower than 2 dB and 3 dB in the 2.45-GHz band. As a result, near the radiation nulls, the SNR is improved by 6 dB. The compact construction and efficient current suppression facilitate the application of HMAs in multi-antenna systems above a finite ground with uniform coverage and reliable connections.

Keywords — Antenna radiation pattern, Characteristic mode analysis, Metamaterials, MIMO communication, Omnidirectional antennas, Wireless access points.

Citation — Bo Zhang, Zhi Ning Chen, Yucong Zhou, *et al*., "Improving radiation pattern roundness of henge-like metaring-loaded monopoles above a finite ground for MIMO systems," *Electromagnetic Science*, vol. 2, no. 2, article no. 0060182, 2024. doi: 10.23919/emsci.2024.0018.

I. Introduction

Multiple-input and multiple-output (MIMO) systems, benefiting from high capacity, reliability, and high data rate, are widely applied in modern wireless networks [1]–[6]. In practical applications, the size of antenna platforms is often constrained by system limitations [7], [8], which becomes even more challenging for systems employing multiple antennas. Consequently, scenarios arise where the antenna-ground system lacks geometric symmetry, either because the antenna is mounted on an irregular platform or positioned off-center on regular/irregular ground. In these scenarios, the electromagnetic wave energy becomes concentrated in a specific area, while the energy in other regions is undesirably weakened. Meanwhile, the distortion results in undesired radiation nulls [9], shown as the blue areas of radiation patterns in Figure 1(a). In low-scattering electromagnetic environments, such as factories, lecture theatres, and stadiums, wireless devices suffer from a notable decline in their communication performance. This decline manifests in various aspects, including reduced signal-to-noise ratio (SNR), capacity, reliability, and increased latency in parts of the access point's (AP) coverage. Improved radiation performance can lead to significant industrial benefits, such as maintaining robust and reliable communication channels, optimizing operational efficiency, and ensuring smooth connectivity for critical applications. In industrial environments, such as factories, where reliable com-

munication is essential for automation and safety systems, omnidirectional radiation pattern can prevent disruptions, enhance productivity, and support the implementation of advanced technologies like Internet of things and real-time data analytics. Therefore, improvements in distorted radiation patterns are not only technical advancements but also vital factors in enabling the reliable and efficient operation of wireless systems in demanding industrial applications.

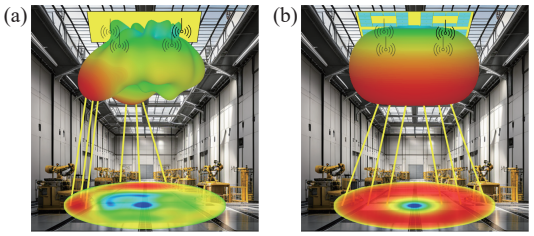

Figure 1 Ceiling-mounted access point coverage for industrial wireless network. (a) Four antennas at the corners of the ground with distorted element radiation patterns and limited coverage; (b) Four henge monopole antennas (HMAs) at the corners of the ground with omnidirectional element radiation patterns and uniform coverage.

Efforts have been devoted to mitigating the pattern distortion of a monopole with irregular boundary conditions. To improve the pattern roundness of an off-center monopole, a metal ring [9] and a metasurface [10] are designed by characteristic mode analysis (CMA) for desired radiation patterns [9]. As radiating structures, they radiate electromagnetic energy within the symmetrical boundary and elevate the mainbeam directions to decouple with the ground. This contributes to suppressing the induced surface currents outside the structures and improves the radiation patterns. However, the relatively bulky size of the structures and their limited efficiency in controlling currents restrict their applications to scenarios where multiple antennas share a finite ground and require omnidirectional radiation patterns. Alternatively, other studies have achieved omnidirectional radiation patterns through progressive feed phase [11]–[14] and polarization diversity [15]–[18]. The former method involves combining radiation patterns of multiple antennas with a progressive feed phase, thereby poses challenges when applied to antennas with four or more ports. The latter approach consumes the resources of orthogonal polarization and presents difficulties when implemented in four or more port MIMO systems.

Based on electromagnetic theory, we can manipulate the roundness of radiation patterns by forming a locally circular symmetric boundary around the monopole on an arbitrary conducting plane. This localizes the ground surface currents and makes the radiation from the monopole irrelevant to the outside environment. Metamaterials are one of the most effective approaches for manipulating electromagnetic waves [19]–[21]. Among them, electromagnetic bandgap (EBG) structures, composed of periodic mushroom unit cells, are widely applied for control ground surface currents in antenna design, such as improving port isolation between patch antennas [22], slot antennas [7], [23], and monopoles [24]. However, encircling antennas with EBG structures causes strong reflected waves and forms strong local resonances, which deteriorates the impedance matching and antenna efficiency. In addition, the mushroom cells also have been used in one dimension as metaline antennas for circular polarization [25], [26], and in two dimensions as metamaterial antennas for low profile [27], wideband [28], and lower back radiation [29].

Inspired by the dual functionality exhibited by mushroom cells, this paper introduces a henge-like metaring (HMR) composed of a single-annular array of mushroom unit cells. The HMR is utilized to encircle a monopole antenna, forming a henge-like monopole antenna (HMA) and establishing symmetric boundaries around off-center monopoles mounted on a finite ground plane. Simulation and measurement results verify the idea with improving the unroundness to less than 3 dB at $\theta = 65°$ plane in the 2.45-GHz band. As a result, the SNR is improved by 6 dB near the radiation nulls of off-center monopoles. The contributions of this paper are as follows:

1) Analysis of pattern distortion. The mechanism of the radiation pattern distortion of off-center monopoles is analyzed. The conclusion shows it is caused by irregular surface currents, which are excited by both the feed and the radiated wave from the monopole, as shown in Figure 2(a).

2) Introduction of HMR with integrated quasi-EBG and radiator functions. To control the irregular surface currents from the two above-mentioned ways, the HMR is proposed with co-designed functions, as shown in Figure 2(b): As a quasi-EBG, it can suppress the surface currents mainly excited by the feed of the monopole. As a radiator, it contributes to elevating the radiation pattern to an upper space, with less coupling with the ground plane, and thus reduces the currents caused by the radiation from the monopole. Meanwhile, a portion of the energy is radiated rather than being reflected to the feed, resulting in enhanced antenna efficiency through improved impedance matching.

3) Four-port MIMO system with improved pattern roundness and communication performance. The proposed MIMO system, composed of four HMAs, achieves omnidirectional radiation pattern of each off-center antenna. The improved radiation pattern contributes to signal power enhancement near the original radiation nulls. Compared with previous works, the proposed MIMO system offers advantages, such as an omnidirectional radiation pattern, a straightforward feeding structure without a power divider, and a configuration accommodating up to four ports. Furthermore, it leaves space for potential enhancements by adding horizontally polarized antennas, thereby opening possibilities to expand the number of antenna ports for higher communication performance.

II. Analysis of Pattern Distortion

Considering the typical scenarios, one monopole is vertically mounted at the center (Case 1) and off-center (Case 2), and four off-center monopoles (Case 3) are symmetrically

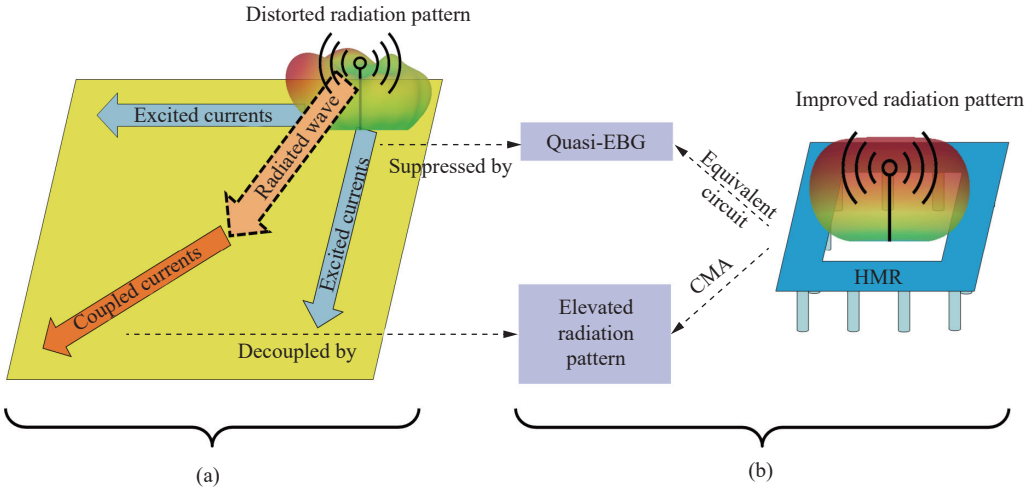

Figure 2 Schematic of (a) Causes of radiation pattern distortion of off-center monopole, (b) The proposed HMR functioning as both quasi-EBG and radiator to improve the radiation pattern.

located on a square ground as shown in Figures 3(a)–(c). Figure 3(d) shows the proposed HMR surrounding the off-center monopole. The square ground plane of both cases is 230 mm × 230 mm or $1.9\lambda_0 \times 1.9\lambda_0$, where λ_0 is the free-space wavelength at 2.45 GHz. The origin of the coordinate is located at the center of the ground. The locations of antennas in Cases 1, 2, and 3 are ($x = 0$, $y = 0$) and ($x = 65$, $y = 65$), ($x = 65$, $y = 65$) and ($x = -65$, $y = 65$), and ($x = 65$, $y = -65$) and ($x = -65$, $y = -65$), respectively, where x and y are in unit of mm.

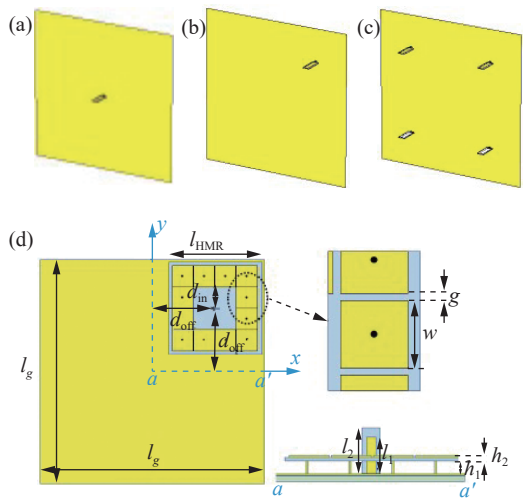

Figure 3 Monopoles mounted on a square ground plane. (a) Case 1: center mounted; (b) Case 2: off-center mounted; (c) Case 3: four mono-poles; (d) Case 2 with the proposed HMR.

To evaluate the symmetry of the radiation pattern, unroundness (UnR) is defined as the maximum gain difference within the cross section of the radiation pattern at a given angle θ_0. Figure 4(a) shows the simulated UnR of Cases 1 and 2 at 2.45 GHz. In Case 1, the monopole with structural symmetry ground reaches a smaller UnR than in Case 2 over all elevation angles. For ceiling-mounted APs, UnR in low elevation angles is of more interest for stable communication links at large distances. Hence, Figure 4(b) shows the UnR in $\theta_0 = 65°$ cutting plane. Case 2 has a UnR of 4.4–5.6 dB against Case 1's UnR of 0.8–2.5 dB over 2.3–2.6 GHz. In the following, the causes of pattern distortion of an off-center monopole are investigated by applying absorbers.

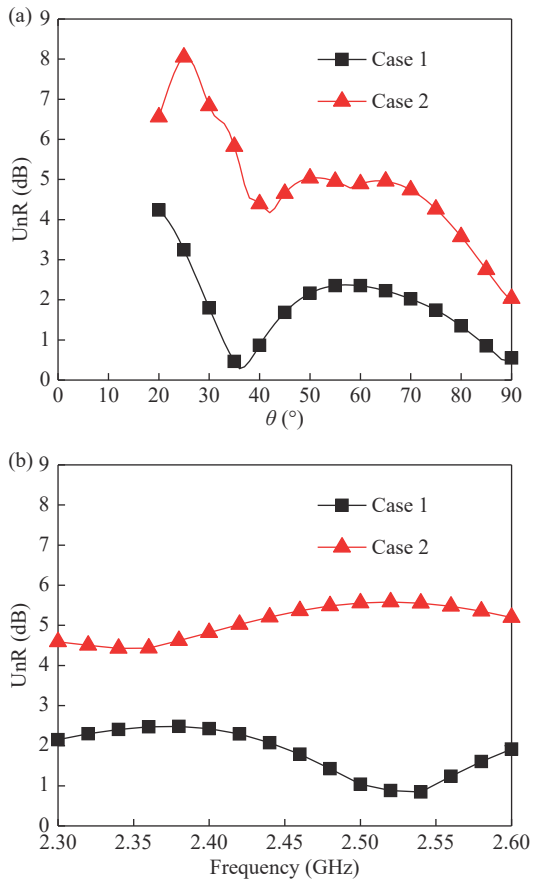

Figure 4 Radiation properties of Case 1 and Case 2. (a) UnR at 2.45 GHz over different θ angles; (b) UnR at $\theta_0 = 65°$ over 2.3–2.6 GHz band.

Assuming Case 2 is partially or totally covered with an absorber sheet (relative permittivity ε_r = relative permeabili-

ty μ_r =10, electric loss tan δ_e = magnetic loss tan δ_m = 0.5) as shown in Figures 5(a) and (b), except for a cylinder area encircling the monopole for effective radiation. Figures 5(c) and (d) present the magnitude of the currents of two cases shown in Figures 5(a) and (b), respectively. It is found that there is no current on the absorbing area of the ground plane, which indicates that the surface currents are fully absorbed by the absorber sheet and cannot travel to the outside ground. Therefore, it is concluded that in the partially covered case, the currents flowing outside of the absorber area are induced by the wave radiated directly from the monopole.

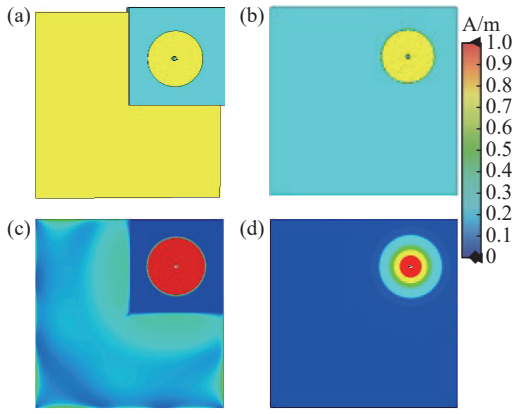

Figure 5 Off-center monopole with absorber surface. (a) Partially covered off-center monopole; (b) Totally covered off-center monopole; (c) Current distribution of partially covered off-center monopole; (d) Current distribution of totally covered off-center monopole. (The light blue part is absorber).

Figure 6 shows the UnR of the monopoles in Figure 5 and a reference monopole as Case 2 in Figure 3(b). The totally covered case provides the lowest UnR in the whole band due to the symmetric current distribution on the ground than the partially covered case. The excited surface currents generated by the monopole's feed have been efficiently absorbed by the surrounding absorber. Consequently, the induction of currents outside the absorber results

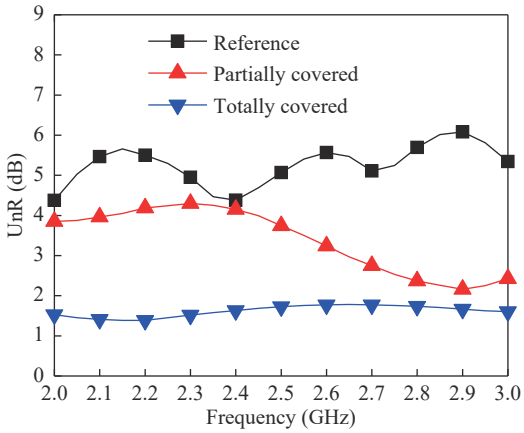

Figure 6 UnR of the off-center monopole without absorber (as the reference), with partially covered absorber, and with totally covered absorber at 2.45 GHz in $\theta_0 = 65°$ plane.

solely from the scattering of the radiated wave produced by the monopole as it interacts with the ground.

Therefore, the radiation pattern of an off-center monopole is distorted by the irregular surface currents excited by both the feed and the wave radiated from the monopole. This finding guides for improving the roundness of an off-center monopole above a finite ground by suppressing the surface currents from both ways simultaneously.

III. Henge-Like Metaring Design

An HMR is designed to control the radiation from surface currents and wave scattering from the ground plane excited by monopoles. The HMR is composed of an annular array of mushroom unit cells. The patches of the cells are suspended above the ground with an air gap. And the vias electrically connect the patches with the ground. The proposed HMR encircling the monopole on the ground localises the surface currents within a symmetric boundary and redirects the main beam to high-elevation angles. Figure 3(d) shows a monopole encircled by an HMR. In the following, the HMR's effects on the antenna's radiation are studied.

1. Quasi-EBG

Periodically arranged mushroom cells are widely applied as EBG structures to suppress surface wave propagation along the ground. The bandgap is addressed by extracting the dispersion curve, where the unit cell is simulated with periodic boundary conditions in two orthogonal dimensions. However, the HMR comprises one column of unit cells along the propagating direction. The dispersion curve cannot accurately predict the stopband of the mushroom unit cells of HMR. Therefore, an equivalent circuit model for one-column mushroom cells, as shown in Figure 7, is proposed and modified by considering the coupling between the monopoles and the mushroom cells [30]. The square patches of the mushroom cells are 21.6 mm in width (w) with a 0.4-mm gap (g) and suspended with a 5.5-mm-thick air gap (h_1), and two monopoles are mounted opposite of the mushroom cells and well-matched at 2.45 GHz. The circuit parameters in the equivalent model shown in Figure 7 are calculated using the formulas in [30] as summarised in Table 1. The one-column mushroom cells are termed quasi-EBG to distinguish from traditional EBG when the HMR functions as a stopband structure.

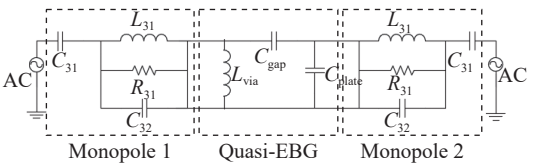

Figure 7 Equivalent circuit of EBG between two monopoles. (AC: alternating current; *R*: resistor; *L*: inductor; *C*: capacitor).

The mushroom unit cells can be designed based on the resonant frequency extracted from the equivalent circuits. When operating at the resonant frequency, the HMR prevents the surface currents from flowing on the ground. As a

Table 1 Values of the components in the equivalent circuit in Figure 7

Component	Value
C_{31} (pF)	0.935
C_{32} (pF)	0.204
L_{31} (nH)	4.3
R_{31} (Ω)	222
C_{gap} (pF)	0.588
C_{plate} (pF)	0.404
L_{via} (nH)	6.9

result, the surface currents are localised by the HMR. However, the reflected surface currents form a strong local resonance as a cavity, deteriorating the impedance matching and antenna efficiency.

2. Radiation from HMR

The HMR can also be applied as a radiator and studied using CMA. The proposed HMR is mounted on an infinite ground, and a monopole is located at the center of the HMR. The modal weighing coefficients (MWCs) of the two most significant modes are shown in Figure 8. The radiating power proportions of the two modes are 66% and 33% of the total radiation power, respectively. Therefore, the radiation pattern of the HMA can be well approximated by the superposition of these two characteristic modes.

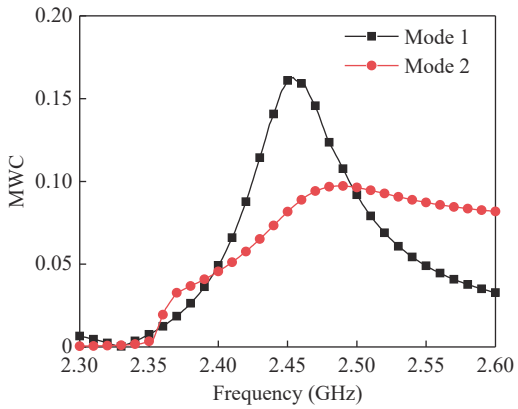

Figure 8 MWC of the HMR with excited monopole on infinite ground plane.

The surface current distribution and the radiation patterns of the HMA are shown in Figure 9. Figures 9(a) and (b) show that the currents on the monopole are strongly excited, and the surface currents are in radial direction from the monopole. Meanwhile, the radiation patterns of Modes 1 and 2 are circularly symmetric and monopole-like, as shown in Figures 9(c) and (d). It indicates that the antenna's radiation pattern will be circularly symmetric if the current distribution of these two modes is circularly symmetric, regardless of the non-circular symmetry of the structure. Furthermore, Figure 9(c) shows that the mainbeam of Mode 1 directs to $\theta_0 = 33°$, while the mainbeam of a monopole above an infinite ground directs to $\theta_0 = 90°$. The elevated radiation ensures less energy coupling to the ground and fewer surface currents induced outside the HMR, contributing to the symmetric pattern of an off-center monopole, as discussed in Section II. Meanwhile, the HMR functions as a radiator, contributing to radiating the energy and mitigating reflected currents from the quasi-EBG functionality, which benefits impedance matching and improves antenna efficiency.

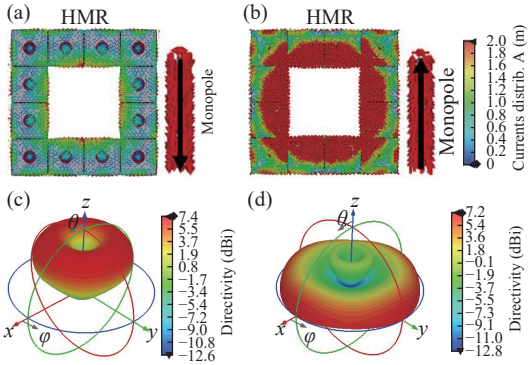

Figure 9 Currents distribution on the HMR and the monopole in (a) Mode 1 and (b) Mode 2. The corresponding radiation pattern of (c) Mode 1 and (d) Mode 2.

On the other hand, for a multi-antenna system, the adjacent monopoles will be illuminated by less energy due to the elevated pattern, which helps to suppress the mutual coupling between antennas. In the following, we will focus on Mode 1, which radiates the majority of power with the desired elevated pattern.

3. Analysis and design

The frequency of the HMR as a quasi-EBG can be calculated by the equivalent circuits, as discussed in Section III.1. As a radiator, the HMR radiates at Mode 1 with MWC reaching the peak, as explained in Section III.2. Figures 10(a) and (b) show the resonance frequencies of quasi-EBG and radiation mode with varying spacing h_1 and width w. It is found that the larger h_1 or w, the lower the resonance frequency of the quasi-EBG. The reason is that the larger spacing h_1 results in larger inductance, and the larger patch width w results in larger capacitance [30]. In the radiation mode, the relation between the geometry size and working frequency of the HMR is similar to a patch antenna [31].

Furthermore, the frequencies with varying patch gap g and width w are given in Figures 10(d) and (e). Figure 10(d) shows that the resonance frequency of HMR as a quasi-EBG monotonically increases as gap g increases [30]. The resonance frequency of the HMR operating at a radiation mode shifts higher since decreased g results in a smaller overall size of the HMR.

In summary, the frequency differences between the quasi-EBG and radiation modes as shown in Figures 10(c) and (f) suggest that the two modes can simultaneously operate at the same frequencies by varying parameters h_1, g, and w. The green regions shown in Figures 10(c) and (f) indicate a convergence of both modes, wherein the surface

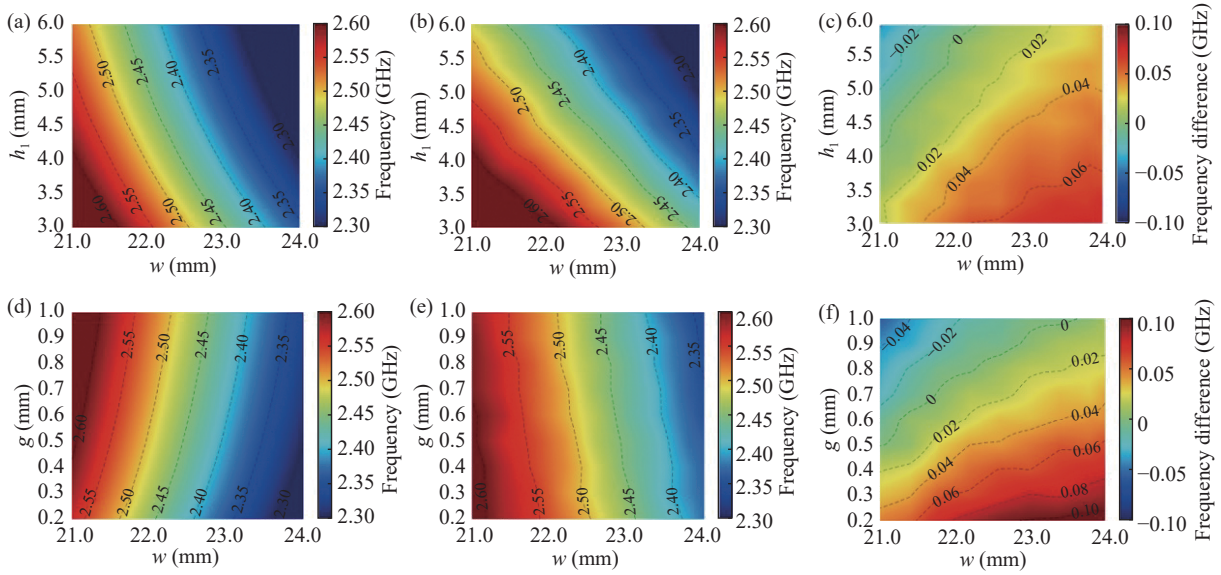

Figure 10 Resonance frequencies of quasi-EBG by equivalent circuit and radiation mode by CMA. (a) Resonance frequency of quasi-EBG with w and h_1; (b) Resonance frequency of radiation mode with w and h_1; (c) Difference between resonance frequency of radiation mode and quasi-EBG with w and h_1; (d) Resonance frequency of quasi-EBG with w and g; (e) Resonance frequency of radiation mode with w and g; (f) Difference between resonance frequency of radiation mode and quasi-EBG with w and g.

currents, excited from the feeding port and induced by the radiation of the monopole antenna, are expected to be suppressed simultaneously.

IV. Antenna Design

1. Single HMA

To verify the proposed HMA, a prototype of a single HMA off-center mounted on a square ground is designed and prototyped as shown in Figure 11(a). The square patches of the mushroom cells are 21.6 mm in width (w) with a 0.4-mm gap (g) and printed on a piece of 0.5-mm-thick Rogers RO4003C substrate, which is suspended with a 5-mm-thick air layer for a wide bandwidth [32]. The surrounding twelve copper vias connect the patches to the ground and support the HMR. The monopole antenna is a 5 mm × 20 mm copper strip printed on a piece of 0.8 mm × 10 mm × 25 mm Rogers RO4003C substrate. The monopole antenna is placed at ($x = d_{off}$, $y = d_{off}$) where d_{off} = 65 mm or $0.53\lambda_0$. The length of the square HMR substrate is l_{HMR} = 95 mm or $0.78\lambda_0$. The distance between the HMR substrate's center and the patches' inner edges is d_{in} = 22.2 mm or $0.18\lambda_0$.

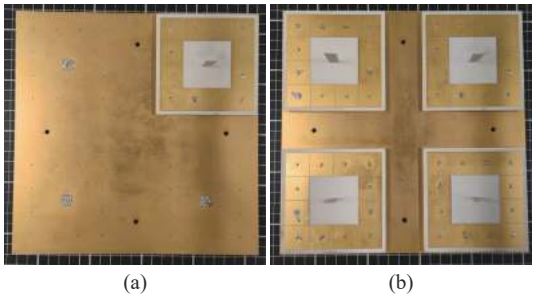

Figure 11 Prototypes of (a) Single off-center mounted HMA and (b) Four off-center mounted HMAs.

Figures 12(a) and (b) compare the simulated surface current distribution of an off-center monopole without and with the HMR. Without the HMR, the surface currents flow over the whole ground plane and concentrate around the two ground edges close to the monopole. The currents at the edges directly distort the radiation pattern, as shown in Figure 12(c), compared with the monopole at the center of the ground. On the contrary, the surface currents outside the HMR are remarkably suppressed while the currents are localised within the HMR, as shown in Figure 12(b). Correspondingly, Figure 12(d) shows a more circularly symmetric radiation pattern because of the much more symmetric localised current distribution than the monopole without the HMR.

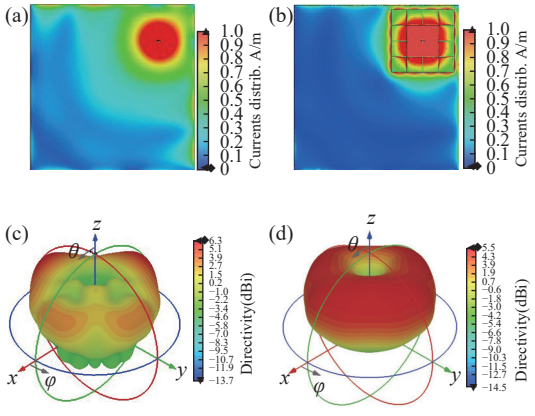

Figure 12 Currents distribution and radiation patterns of off-center monopole with and without HMR. (a) Currents distribution without HMR; (b) Currents distribution with HMR; (c) Radiation pattern without HMR; (d) Radiation pattern with HMR.

The symmetric radiation pattern can be illustrated by combining the radiation mode and quasi-EBG of the HMR,

as discussed in Section III. First, the spreading of surface currents is suppressed when encountering the HMR.

Therefore, relatively strong currents localised within a symmetric ground area encircled by an HMR mainly contribute to a symmetric radiation pattern. Second, the HMR operates as a metaline antenna radiating from its edges, whose characteristic mode radiates with an elevated pattern in the upper space. This is verified by comparing the mainbeam direction of Figures 12(c) and (d). The mainbeam points to $\theta_0 = 59°$, while the HMA radiates to $\theta_0 = 45°$. The elevated pattern, designed for reduced coupling with the ground, effectively mitigates ground-induced scattering. As a result, the antenna's radiation pattern is less susceptible to distortion from the irregular ground.

Figure 13 shows the simulated and measured reflection coefficients of the prototype. Both the monopoles show impedance matching within the 2.45-GHz WLAN band. The reflection coefficient ($|S_{11}|$) of the HMA shows a significant difference with the unloaded monopole because the HMR works as both radiator and quasi-EBG. By tuning the height of the monopole, the HMA reaches impedance matching. The dip of $|S_{11}|$ is caused by the well-excited Mode 1 as analysed in Section III. Meanwhile, $|S_{11}|$ response at the upper band is caused by another well excited characteristic Mode 2. With the end-fire radiation pattern, the operation of Mode 2 is more easily affected by the ground perturbation, such as the ground edges. Therefore, the radiation pattern deteriorates at the upper edge band.

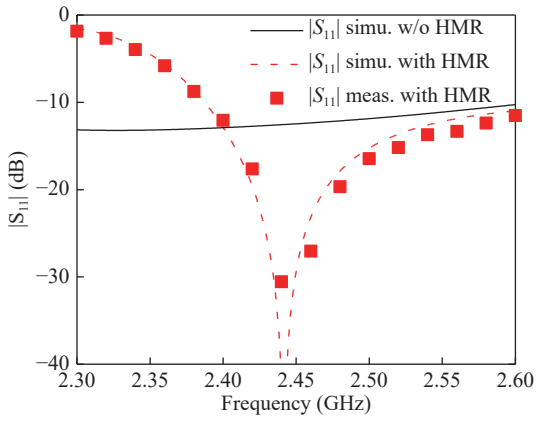

Figure 13 Simulated and measured $|S_{11}|$ of off-center monopole with and without HMR. (simu. stands for simulation, meas. for measured, w/o for without).

To further evaluate the radiation performance of the HMA, some radiation features are shown in Figure 14. In Figure 14(a), the UnR is plotted with different θ angles at 2.45 GHz. It can be found the HMR reduces the UnR in almost the whole upper space of the ground plane. The radiation pattern in $\theta_0 = 65°$ plane at 2.45 GHz is presented in Figure 14(b). This evaluation angle is selected because the UnR performance shows a more important role in larger θ angles of a monopole antenna in AP applications for stable communication coverage of far-zone users. The HMA achieves the UnR of 1.2 dB and 1.4 dB in simulation and

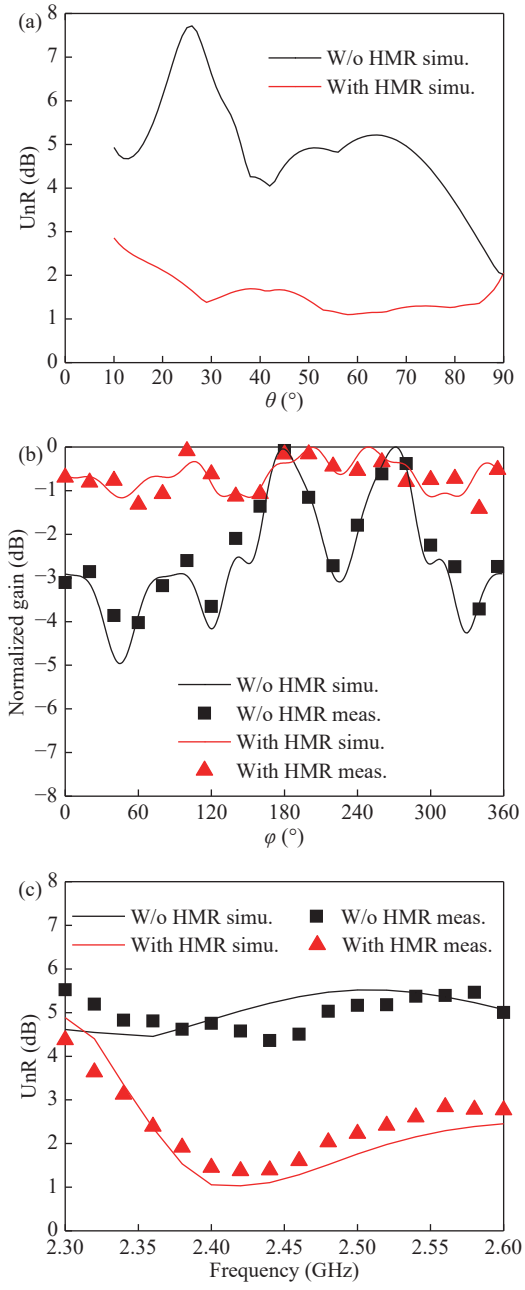

Figure 14 (a) Simulated UnR of one off-center monopole with and without HMR in upper half space at 2.45 GHz; (b) Simulated and measured normalized radiation patterns of off-center monopole with and without HMR at 2.45 GHz in $\theta_0 = 65°$ plane; (c) Simulated and measured UnR of off-center monopole with and without HMR in $\theta_0 = 65°$ plane. (simu. stands for simulation, meas. for measured).

measurement when the UnR of a monopole without the HMR is 5.0 dB and 4.3 dB, respectively. The UnR is improved by 76% and 67% using the proposed HMR. Assembly errors mainly cause the difference between simulated and measured results. Moreover, the UnR performance in $\theta_0 = 65°$ plane at the 2.45 GHz band is presented in Figure 14(c). The HMA achieves a maximum UnR of less than 1.5 dB and 2.0 dB in simulation and measurement within the bandwidth, respectively. More than 3 dB UnR improvement is realized compared with the monopole without HMR.

2. Four HMAs

The four HMAs are used to form a four-antenna MIMO system, as shown in Figure 11(b). The HMAs are mounted at the four corners of a square ground with the same off-center distance as the single HMA. And the minimum edge-to-edge spacing between two HMRs is 35 mm or $0.29\lambda_0$.

The *S*-parameters of the four-monopole antenna system with and without the HMRs are shown in Figure 15. The measured $|S_{11}|$ of the proposed antenna is less than −10 dB in the 2.45 GHz WLAN band with a slight frequency shift referenced to the simulated results because of the fabrication tolerance. Meanwhile, the mutual coupling between the adjacent HMAs ($|S_{21}|$) is less than −32 dB in the 2.45 GHz wireless local-area network (WLAN) band, at least 14 dB lower compared with the unloaded monopoles. It suggests that the HMRs function as a quasi-EBG and lowers the mutual coupling between adjacent monopoles. Meanwhile, the port isolation between two diagonal monopoles ($|S_{31}|$) is enhanced by 11 dB, and the dip shifts to around 2.32 GHz as shown in Figure 15. The reason is that the coupling path between two diagonally placed monopoles is inclined with the HMR columns. And when the wave obliquely incidents on the HMR, the travelling path of the wave is longer than analyzed. Therefore, the equivalent capacitor is enlarged, and the frequency is shifted to a lower frequency [32].

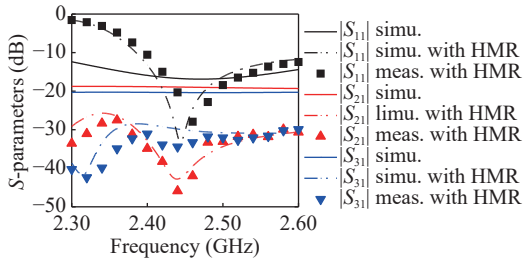

Figure 15 Simulated and measured *S*-parameters of four off-center monopoles with and without HMRs.

Figure 16(a) shows UnR of one antenna in the MIMO antennas is reduced in the upper space of ground plane at 2.45 GHz by applying the HMRs. Figures 16(b) and (c) present the radiation patterns at 2.45 GHz and the wideband performance of the UnR in $\theta_0 = 65°$ plane. The UnR is kept lower than 3 dB in the 2.45 GHz band. Compared with a single HMA, the UnR deteriorates to 2.8 dB at 2.45 GHz due to the coupling between the outer edges of HMRs .

3. Comparison and discussion

Table 2 compares our design with the other designs. For multiple antennas sharing the same finite ground, most of the works try to alleviate the ground effect by combining the radiation patterns of multiple radiation elements with the center of the whole geometry located at the center of the ground [10]–[13], [15], [16]. Then diversity can be achieved by feeding with progressive phase [10]–[13] and orthogonal polarization [15], [16]. Additional power dividers and phase shift lines are required for the progressive feeding phase and combining the radiation patterns from multiple antennas, which is limited to 2 or 3 ports design rather than MIMO antenna systems. For polarization diversity [15], [16], the center-mounted antennas can achieve omnidirectional radiation patterns with little influence by the orthogonally polarized antennas and the ground. However, it is difficult to further increase the number of antenna ports while keeping the omnidirectional patterns for improving MIMO performance. Thus, researchers have de-

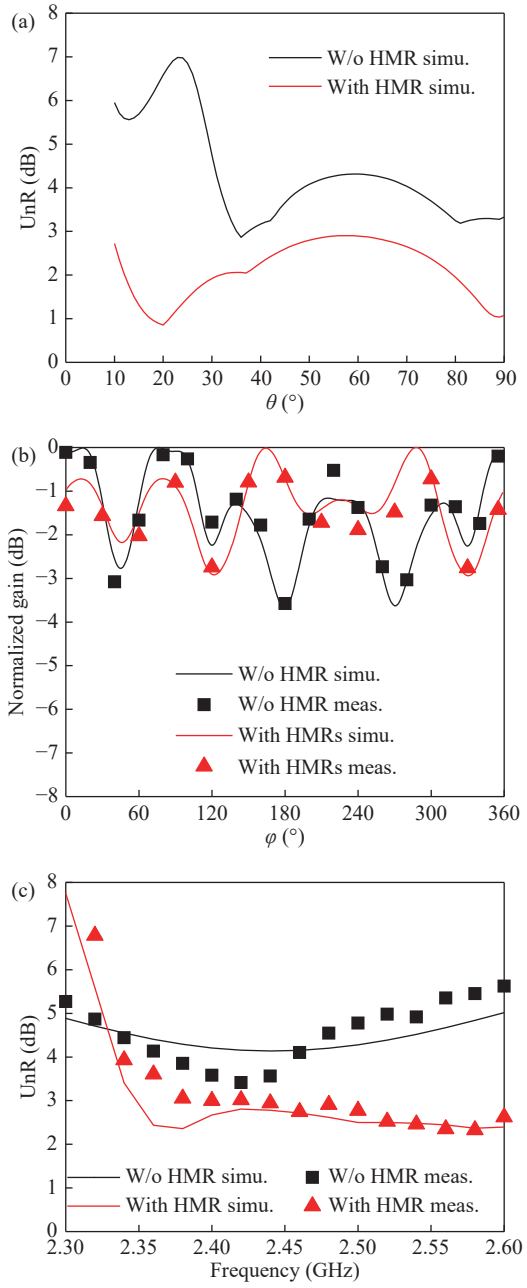

Figure 16 (a) Simulated UnR of four off-center monopoles with and without HMRs in upper half space at 2.45 GHz; (b) Simulated and measured normalized radiation pattern of four off-center monopoles with and without HMRs at 2.45 GHz in $\theta_0 = 65°$ plane; (c) Simulated and measured UnR of four off-center monopoles with and without HMRs in $\theta_0 = 65°$ plane.

signed MIMO antenna systems with one- or two-ports off-center antennas with round radiation patterns [9], [18]. Compared with the works mentioned above, the proposed design achieves a four-port MIMO antenna system with omnidirectional radiation patterns above the ground. Besides, this work has focused on improving the radiation patterns of the vertically polarized antennas since they are more affected by the ground, and it leaves space for horizontally polarized antennas to further increase the number of ports and improve the MIMO performance.

Table 2 Comparisons of various omnidirectional MIMO antennas

Ref.	Technique	Antenna center location on ground plane	Polarization	Number of ports	Power divider	Max UnR (dB)
[10]	Radiation pattern phase	Center	VP	2	Yes	5^{*1}
[11]	Radiation pattern phase	Center	HP	2	Yes	3.4^{*1}
[12]	Radiation pattern phase	Center	VP	2	Yes	3.2^{*1}
[13]	Radiation pattern phase	Center	VP	3	Yes	3.4^{*1}
[15]	Polarization	Center	VP, HP	2	No	3.5^{*1}
[16]	Polarization	Center	VP, HP	2	Yes	NG
[9]	CMA	Off-center	VP	1	No	1.2^{*2}
[10]	CMA, metasurface	Off-center	VP	2	No	2^{*2}
Proposed	EBG, CMA, metaring	Off-center	VP	4	No	1.1^{*1} 2.4^{*2} 3^{*3}

Note: ^{*1}The UnR is evaluated at $\theta_0 = 90°$ plane. ^{*2}The UnR is evaluated at H-plane. ^{*3}The UnR is evaluated at $\theta_0 = 65°$ plane.

4. Effects on communication link performance

Industrial wireless networks necessitate stringent requirements for achieving high-quality communication links. This subsection analyses the effects of the radiation pattern roundness of antennas on communication performance.

The normalized radiation patterns in the upper space ($z > 0$) of the single and multiple antennas without HMR are plotted in Figures 17(a) and (d). Two radiation nulls are observed at −11 dB around $\theta = 26°$, $\varphi = 186°$, and $\theta = 26°$, $\varphi = 264°$ for the single off-center monopole, as depicted in Figure 17(a). Similarly, the MIMO system in Figure 17(d) exhibits radiation nulls at −14 dB around $\theta = 23°$, $\varphi = 184°$, and $\theta = 23°$, $\varphi = 266°$. The presence of radiation nulls, resulting from the irregularities in the surrounding environment, diminishes signal power for users, reduces SNR, degrades channel capacity and reliability, as well as increases latency. These factors collectively impact the overall performance of the system, introducing challenges that need to be addressed to ensure efficient and reliable communication within industrial wireless networks.

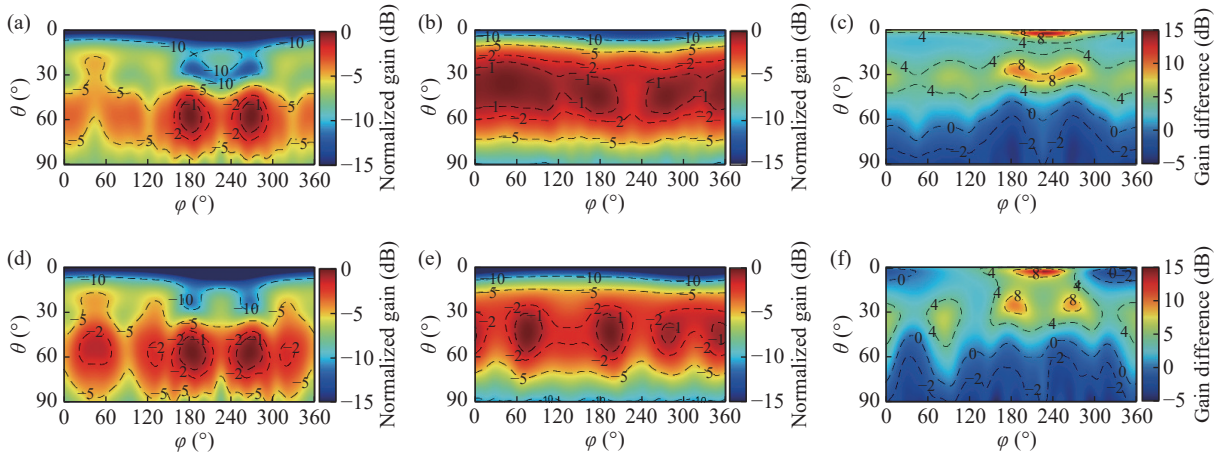

Figure 17 2D-radiation patterns and the gain differences. (a) and (d) Radiation patterns of an off-center monopole in the single- and four-antenna system; (b) and (e) Radiation patterns of an off-center HMA in the single- and four-antenna system; (c) and (f) Gain differences of the off-center HMA and monopole in the single- and four-antenna systems.

With the proposed HMR, the normalized radiation pattern presents near uniform radiation patterns along azimuth cutting planes both for single- and four-antenna systems, as shown in Figures 17(b) and (e). Accordingly, the gain is improved by 9.7 dB for the single-antenna system and 9.5 dB for the four-antenna system at the corresponding null areas,

as shown in Figures 17(c) and (f). Besides, within the AP coverage angles ($\theta < 65°$), the gain is averagely improved by 3.4 dB for the single-antenna system and 2.8 dB for the four-antenna system. The increased radiation power within the effective coverage area of the AP enhances the communication link quality within the area while mitigating interference with other wireless devices located outside the area.

To validate the positive impact of improved radiation pattern roundness on communication performance, experiments were conducted using 4-quadratic-amplitude modulation (4-QAM) modulation. Figure 18 shows the measured constellation map of the off-center monopole antennas with and without the proposed HMRs in the IQ space. For the off-center antenna without HMR, the scattering and displacement of the points indicates the low power of the signal and high signal error rates. After applying the HMR, the points are more concentrated near the ideal points.

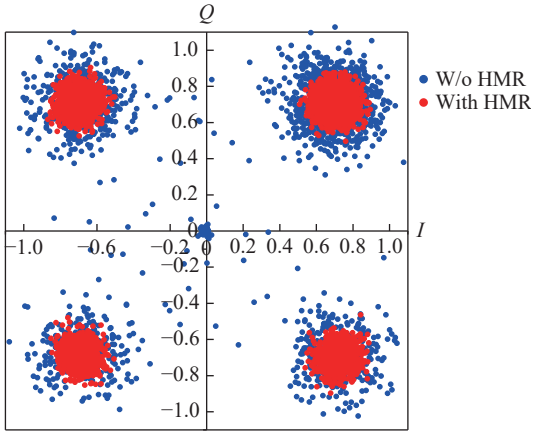

Figure 18 Measured constellation map of off-center monopole antennas with and without the proposed HMRs.

Accordingly, the SNR among received signal samples was also measured as shown in Figure 19. The proposed implementation yields a significant average increase of 6 dB. Despite the additional cost for fabricating the vias and tuning impedance matching, this enhancement ensures a more stable and reliable performance for communication systems.

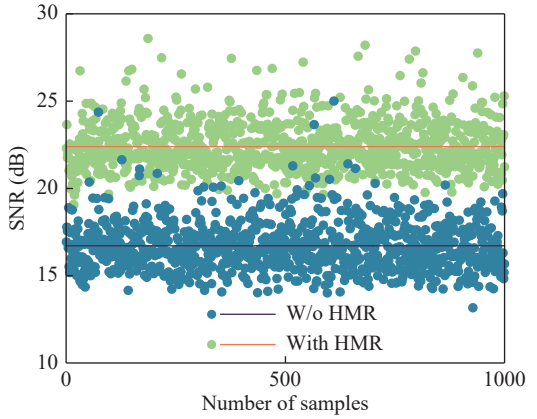

Figure 19 Measured SNR near the radiation nulls of the off-center monopole antennas with and without HMR. Dots for samples and solid lines for average values.

V. Conclusion

An HMR has been proposed to combine quasi-EBG and radiation mode to control the radiation patterns of monopoles off-center situated on a finite-sized ground plane. Analysis has concluded that the asymmetrical currents induced by both the excitation and the radiated field of the monopole contribute to the distortion of radiation patterns. The study has also shown that the symmetric HMR has performed as a quasi-EBG to localize the surface currents in a desired symmetric boundary and an antenna to radiate with an elevated pattern resulting in less coupling with the ground plane. Two designs have verified the design method. The simulation and measurement show that the designed off-center HMAs above a ground plane have achieved uniform coverage with lower than 2 dB and 3 dB UnR of the single- and four-antenna element patterns in $\theta_0 = 65°$ plane. Meanwhile, near the direction of the radiation nulls, the SNR is improved by 6 dB. The proposed HMR can be applied to control radiation patterns in much more scenarios of industrial wireless networks with stable and reliable communication.

Acknowledgements

The authors would like to thank Mr. Yi Chen from Huawei Technologies Co., Ltd., Shenzhen, China, for fruitful discussions, Dr. Terence S. P. See from the Institute for Infocomm Research (I^2R), Singapore, for assistance in measurements, and financial support from Huawei Technologies Co., Ltd., Shenzhen, China

References

[1] B. Liu, X. Yi, K. T. Yang, *et al.*, "A carrier aggregation transmitter front end for 5-GHz WLAN 802.11ax Application in 40-nm CMOS," *IEEE Transactions on Microwave Theory and Techniques*, vol. 68, no. 1, pp. 264–276, 2020.

[2] B. Liu, X. Quan, C. C. Boon, *et al.*, "Reconfigurable 2.4-/5-GHz dual-band transmitter front-end supporting 1024-QAM for WLAN 802.11ax application in 40-nm CMOS," *IEEE Transactions on Microwave Theory and Techniques*, vol. 68, no. 9, pp. 4018–4030, 2020.

[3] K. Hausmair, S. Gustafsson, C. Sanchez-Perez, *et al.*, "Prediction of nonlinear distortion in wideband active antenna arrays," *IEEE Transactions on Microwave Theory and Techniques*, vol. 65, no. 11, pp. 4550–4563, 2017.

[4] C. Karnfelt, P. Hallbjorner, H. Zirath, *et al.*, "High gain active microstrip antenna for 60-GHz WLAN/WPAN applications," *IEEE Transactions on Microwave Theory and Techniques*, vol. 54, no. 6, pp. 2593–2603, 2006.

[5] M. Li, Y. J. Zhang, F. Jiang, *et al.*, "Improvement for MIMO systems by increasing antenna isolation and shaping radiation pattern using hybrid network," *IEEE Transactions on Industrial Electronics*, vol. 69, no. 12, pp. 13891–13901, 2022.

[6] H. R. Chuang and L. C. Kuo, "3-D FDTD design analysis of a 2.4-Ghz polarization-diversity printed dipole antenna with integrated balun and polarization-switching circuit for WLAN and wireless communication applications," *IEEE Transactions on Microwave Theory and Techniques*, vol. 51, no. 2, pp. 374–381, 2003.

[7] G. H. Zhai, Z. N. Chen, and X. Qing, "Mutual coupling reduction of

a closely spaced four-element MIMO antenna system using discrete mushrooms," *IEEE Transactions on Microwave Theory and Techniques*, vol. 64, no. 10, pp. 3060–3067, 2016.

[8] S. R. Best, "The significance of ground-plane size and antenna location in establishing the performance of ground-plane-dependent antennas," *IEEE Antennas and Propagation Magazine*, vol. 51, no. 6, pp. 29–43, 2009.

[9] H. W. Sheng and Z. N. Chen, "Improving radiation pattern roundness of a monopole antenna placed off-center above a circular ground plane using characteristic mode analysis," *IEEE Transactions on Antennas and Propagation*, vol. 69, no. 2, pp. 1135–1139, 2021.

[10] H. W. Sheng and Z. N. Chen, "Metasurface-loaded off-center monopoles with wideband radiation performance using characteristic mode analysis," *IEEE Transactions on Antennas and Propagation*, vol. 70, no. 11, pp. 10660–10668, 2022.

[11] R. N. Lian, T. Y. Shih, Y. Z. Yin, *et al*., "A high-isolation, ultra-wideband simultaneous transmit and receive antenna with monopole-like radiation characteristics," *IEEE Transactions on Antennas and Propagation*, vol. 66, no. 2, pp. 1002–1007, 2018.

[12] L. B. Sun, Y. Li, Z. J. Zhang, *et al*., "A compact planar omnidirectional MIMO array antenna with pattern phase diversity using folded dipole element," *IEEE Transactions on Antennas and Propagation*, vol. 67, no. 3, pp. 1688–1696, 2019.

[13] D. Wu, Y. Z. Zang, H. Luyen, *et al*., "A compact, low-profile simultaneous transmit and receive antenna with monopole-like radiation characteristics," *IEEE Antennas and Wireless Propagation Letters*, vol. 18, no. 4, pp. 611–615,Apr, 2019.

[14] C. J. Deng, B. L. Shi, and D. Liu, "Compact omnidirectional three-port MIMO antenna with the same vertical polarization for WLAN applications," *Microwave and Optical Technology Letters*, vol. 62, no. 2, pp. 800–805, 2020.

[15] Y. Li, Z. J. Zhang, Z. H. Feng, *et al*., "Design of omnidirectional dual-polarized antenna in slender and low-profile column," *IEEE Transactions on Antennas and Propagation*, vol. 62, no. 4, pp. 2323–2326, 2014.

[16] J. L. Wu, S. W. Yang, Y. K. Chen, *et al*., "A low profile dual-polarized wideband omnidirectional antenna based on AMC reflector," *IEEE Transactions on Antennas and Propagation*, vol. 65, no. 1, pp. 368–374, 2017.

[17] Z. Wang, Y. W. Ning, and Y. D. Dong, "Hybrid metamaterial-TL-based, low-profile, dual-polarized omnidirectional antenna for 5G indoor application," *IEEE Transactions on Antennas and Propagation*, vol. 70, no. 4, pp. 2561–2570, 2022.

[18] S. B. Liu, F. S. Zhang, M. Boyuan, *et al*., "Multiband dual-polarized hybrid antenna with complementary beam for simultaneous RF energy harvesting and WPT," *IEEE Transactions on Antennas and Propagation*, vol. 70, no. 9, pp. 8485–8495, 2022.

[19] J. W. You, Q. Ma, L. Zhang, *et al*., "Electromagnetic metamaterials: From classical to quantum," *Electromagnetic Science*, vol. 1, no. 1, article no. 0010051, 2023.

[20] B. Zheng, H. Lu, C. Qian, *et al*., "Revealing the transformation invariance of full-parameter omnidirectional invisibility cloaks," *Electromagnetic Science*, vol. 1, no. 2, article no. 0020092, 2023.

[21] J. C. Zhang, G. B. Wu, M. K. Chen, *et al*., "Electromagnetic wave tailoring: From one dimension to multiple dimensions," *Electromagnetic Science*, vol. 1, no. 3, article no. 0030131, 2023.

[22] F. Yang and Y. Rahmat-Samii, "Microstrip antennas integrated with electromagnetic band-gap (EBG) structures: A low mutual coupling design for array applications," *IEEE Transactions on Antennas and Propagation*, vol. 51, no. 10, pp. 2936–2946, 2003.

[23] G. H. Zhai, Z. N. Chen, and X. Qing, "Enhanced isolation of a closely spaced four-element MIMO antenna system using metamaterial mushroom," *IEEE Transactions on Antennas and Propagation*, vol. 63, no. 8, pp. 3362–3370, 2015.

[24] D. A. Ketzaki and T. V. Yioultsis, "Metamaterial-based design of planar compact MIMO monopoles," *IEEE Transactions on Antennas and Propagation*, vol. 61, no. 5, pp. 2758–2766, 2013.

[25] H. Nakano, T. Abe, and J. Yamauchi, "A small metaline array antenna for circularly polarized dual-band beam-steering," *IEEE Access*, vol. 10, pp. 73317–73325, 2022.

[26] H. Nakano, T. Abe, and J. Yamauchi, "Planar reconfigurable antennas using circularly polarized metalines," *IEEE Antennas and Wireless Propagation Letters*, vol. 18, no. 5, pp. 1006–1010, 2019.

[27] W. Liu, Z. N. Chen, and X. Qing, "Metamaterial-based low-profile broadband mushroom antenna," *IEEE Transactions on Antennas and Propagation*, vol. 62, no. 3, pp. 1165–1172, 2014.

[28] W. Liu, Z. N. Chen, and X. Qing, "Low-profile broadband antennas using metamaterial-mushroom structures (invited)," in *Proceedings of the 2015 IEEE International Conference on Computational Electromagnetics*, Hong Kong, China, pp. 33–34, 2015.

[29] W. Liu, Z. N. Chen, and X. Qing, "Stripline aperture coupled metamaterial mushroom antenna with increased front-to-back ratio," in *Proceedings of the IEEE Antennas and Propagation Society International Symposium (APSURSI)*, Memphis, TN, USA, pp. 444–445, 2014.

[30] A. S. Arman, M. Ali, and T. R. Vogler, "A simple technique for EBG design for monopole antenna isolation improvement," in *Proceedings of the 2019 IEEE International Symposium on Antennas and Propagation and USNC-URSI Radio Science Meeting*, Atlanta, USA, pp. 1177–1178, 2019.

[31] Z. N. Chen, D. X. Liu, H. Nakano, *et al*., *Handbook of Antenna Technologies*. Springer, Singapore, 2016.

[32] F. Yang and Y. Rahmat-Samii, *Electromagnetic Band Gap Structures in Antenna Engineering*. Cambridge University Press, Cambridge, UK, 2008.

Bo Zhang received the B.S. degree from University of Electronic Science and Technology of China, Chengdu, China, and the M.S. degree from National University of Singapore, Singapore, in 2019 and 2020, respectively. He is currently pursuing the Ph.D. degree at the Department of Electrical and Computer Engineering, National University of Singapore, Singapore. His current research interests include antenna radiation pattern, metamaterials, metasurfaces, and multi-input multi-output antennas. (Email: bzhang@u.nus.edu)

Zhi Ning Chen received the B.E., M.E., and Ph.D. degrees from the Institute of Communications Engineering, Beijing, China, in 1985, 1988, and 1993, respectively, and the second Ph.D. degree from the University of Tsukuba, Tsukuba, Japan, in 2003. He is working at the Department of Electrical and Computer Engineering, National University of Singapore, Singapore, as a Provost Chair Professor and the Director of Advanced Research and Technology Innovation Centre. Dr. Chen has published more that 720 academic papers and six books. Recently he has focused more on the translational research and technology development of metantennas and algorithm-based antenna design (prior-knowledge-guided machine learning-enabled synthesis and optimization). (Email: eleczn@nus.edu.sg)

Yucong Zhou received the B.S. and Ph.D. degrees from University of Electronic Science and Technology of China, Chengdu, China, in 2010 and 2016, respectively. He jointed Huawei Technology Co., Ltd., Shenzhen, China, in 2016. Currently, he is a Technical Research Engineer in Huawei's Fourier Lab, Chengdu, China, focusing on WLAN antenna technology research. (Email: zhouyucong@huawei.com)

Qun Lou received the Ph.D. degree in electronic science and technology from Nanjing University, Nanjing, China, in 2018, and was a research fellow at National University of Singapore, Singapore, during 2018 to 2023. From 2023, he joined South China Agricultural University, Guangzhou, China, as an Associate Professor. His current research interests include metasurfaces, metamaterials, photonic crystals, and new technologies in antenna designs.
(Email: elelouq@nus.edu.sg)

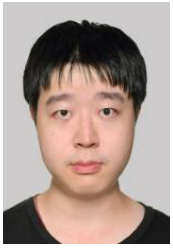

Jiahao Wang received the B.S. degree in communication engineering from University of Electronic Science and Technology of China, Chengdu, China, in 2018. He is currently pursuing the Ph.D. degree at the College of Design and Engineering, National University of Singapore, Singapore. His research interests include communication technology, conformal antenna array design and analysis, direction of arrival estimation, and beamforming techniques.
(Email: jiahaowang@u.nus.edu)

Koen Mouthaan received the M.S. and Ph.D. degrees in electrical engineering from Delft University of Technology, Delft, Netherlands. He worked at TNO Defense, Safety and Security in the Netherlands, and at SkyGate, a company that designed phased-array antennas for consumer applications. During 2003 and 2015, he was an Assistant Professor and an Associate Professor with the Department of Electrical and Computer Engineering, National University of Singapore, Singapore. He rejoined the same department in 2016. His research interests include microwave and millimeter-wave circuits and systems, phased array antennas, digital beamforming, design and innovation. He also received an MBA degree from Nanyang Technological University, Singapore, a M.S. degree in organizational leadership from Johns Hopkins University, Baltimore, MD, USA, and a M.S. degree in space engineering from the Technical University of Berlin, Berlin, Germany.
(Email: k.mouthaan@nus.edu.sg)